

University of Dundee

Polyubiquitin binding to ABIN1 is required to prevent autoimmunity

Nanda, Sambit K.; Venigalla, Ram K. C.; Ordureau, Alban; Patterson-Kane, Janet C.; Powell, David W.; Toth, Rachel

Published in:
Journal of Experimental Medicine

DOI:
[10.1084/jem.20102177](https://doi.org/10.1084/jem.20102177)

Publication date:
2011

Document Version
Publisher's PDF, also known as Version of record

[Link to publication in Discovery Research Portal](#)

Citation for published version (APA):
Nanda, S. K., Venigalla, R. K. C., Ordureau, A., Patterson-Kane, J. C., Powell, D. W., Toth, R., Arthur, J. S. C., & Cohen, P. (2011). Polyubiquitin binding to ABIN1 is required to prevent autoimmunity. *Journal of Experimental Medicine*, 208(6), 1215-1228. <https://doi.org/10.1084/jem.20102177>

General rights

Copyright and moral rights for the publications made accessible in Discovery Research Portal are retained by the authors and/or other copyright owners and it is a condition of accessing publications that users recognise and abide by the legal requirements associated with these rights.

- Users may download and print one copy of any publication from Discovery Research Portal for the purpose of private study or research.
- You may not further distribute the material or use it for any profit-making activity or commercial gain.
- You may freely distribute the URL identifying the publication in the public portal.

Take down policy

If you believe that this document breaches copyright please contact us providing details, and we will remove access to the work immediately and investigate your claim.

Polyubiquitin binding to ABIN1 is required to prevent autoimmunity

Sambit K. Nanda,¹ Ram K.C. Venigalla,¹ Alban Ordureau,¹ Janet C. Patterson-Kane,² David W. Powell,³ Rachel Toth,¹ J. Simon C. Arthur,¹ and Philip Cohen¹

¹Medical Research Council Protein Phosphorylation Unit, Sir James Black Centre, University of Dundee, Dundee DD1 5EH, Scotland, UK

²Veterinary Diagnostic Services, School of Veterinary Medicine, College of Medical, Veterinary and Life Sciences, University of Glasgow, Glasgow G61 1QH, UK

³Department of Medicine and Biochemistry and Molecular Biology, University of Louisville School of Medicine, Louisville, KY 40202

The protein ABIN1 possesses a polyubiquitin-binding domain homologous to that present in nuclear factor κ B (NF- κ B) essential modulator (NEMO), a component of the inhibitor of NF- κ B (I κ B) kinase (IKK) complex. To address the physiological significance of polyubiquitin binding, we generated knockin mice expressing the ABIN1[D485N] mutant instead of the wild-type (WT) protein. These mice developed all the hallmarks of autoimmunity, including spontaneous formation of germinal centers, isotype switching, and production of autoreactive antibodies. Autoimmunity was suppressed by crossing to MyD88^{-/-} mice, demonstrating that toll-like receptor (TLR)-MyD88 signaling pathways are needed for the phenotype to develop. The B cells and myeloid cells of the ABIN1[D485N] mice showed enhanced activation of the protein kinases TAK, IKK- α/β , c-Jun N-terminal kinases, and p38 α mitogen-activated protein kinase and produced more IL-6 and IL-12 than WT. The mutant B cells also proliferated more rapidly in response to TLR ligands. Our results indicate that the interaction of ABIN1 with polyubiquitin is required to limit the activation of TLR-MyD88 pathways and prevent autoimmunity.

CORRESPONDENCE

Philip Cohen:
p.cohen@dundee.ac.uk
OR
Sambit K. Nanda:
s.k.nanda@dundee.ac.uk

Abbreviations used: ABIN, A20-binding inhibitor of NF- κ B; BCR, B cell receptor; BMDM, BM-derived macrophage; ICOS, inducible co-stimulator; I κ B, inhibitor of NF- κ B; IKK, I κ B kinase; IRAK, IL-1 receptor-associated kinase; JNK, c-Jun N-terminal kinase; LTA, lipoteichoic acid; MAPK, mitogen-activated protein kinase; NEMO, NF- κ B essential modulator; NOD, nucleotide oligomerization domain; PAS, periodic acid-Schiff; T_H cell, follicular helper T cell; TLR, Toll-like receptor; TRAF, TNF receptor-associated factor; T reg cell, regulatory T cell; UBAN, ubiquitin-binding domain in ABIN and NEMO.

The activation of the innate immune system involves a complex interplay between protein phosphorylation and protein ubiquitylation events. For example, the activation of Toll-like receptors (TLRs) that signal through the adaptor protein MyD88 switches on protein kinases, such as IL-1 receptor-associated kinases (IRAKs), and E3 ubiquitin ligases, such as TNF receptor-associated factor (TRAF) 6 (Walsh et al., 2008) and Pellino (Ordureau et al., 2008). These E3 ligases are then thought to induce the formation of Lys63-linked polyubiquitin (K63-pUb) chains, which may be linked covalently to other proteins, such as IRAK1 and TRAF6 (Wang et al., 2001; Conze et al., 2008; Windheim et al., 2008), or may not be anchored to any other protein (Xia et al., 2009).

The K63-pUb chains and K63-pUb-proteins regulate downstream signaling pathways by interacting with polyubiquitin-binding proteins that include the regulatory components of other protein kinases. For example, the binding of K63-pUb chains to the TAB2 and TAB3 components of the TAK1 complex (Kanayama et al., 2004; Kulathu et al., 2009;

Sato et al., 2009) induces a conformational change that activates this protein kinase (Xia et al., 2009), enabling TAK1 to initiate activation of the canonical inhibitor of NF- κ B (I κ B) kinase (IKK) complex. The NF- κ B essential modulator (NEMO) component of the canonical IKK complex also binds to K63-pUb chains, and mutations that abrogate its binding to polyubiquitin (e.g., NEMO[D311N]) prevent activation of the IKKs (Ea et al., 2006; Wu et al., 2006) and NF- κ B-dependent gene transcription (Windheim et al., 2008) in response to inflammatory stimuli and cause immunodeficiency in man (Döflinger et al., 2001). These findings imply that the binding of polyubiquitin to NEMO is required for activation of the canonical IKKs, as well as the activation of TAK1. The K63-pUb chains may act as scaffolds to colocalize the IKK complex with TAK1, and/or their interaction with NEMO

© 2011 Nanda et al. This article is distributed under the terms of an Attribution-Noncommercial-Share Alike-No Mirror Sites license for the first six months after the publication date (see <http://www.rupress.org/terms>). After six months it is available under a Creative Commons License (Attribution-Noncommercial-Share Alike 3.0 Unported license, as described at <http://creativecommons.org/licenses/by-nc-sa/3.0/>).

may induce a conformational change that facilitates phosphorylation of the activation loop of the canonical IKKs by TAK1 and/or autophosphorylation.

The canonical IKKs activate NF- κ B by phosphorylating the inhibitory I κ B α component of this transcription factor, which marks I κ B α for K48-linked polyubiquitylation by the SCF^{TRCP} E3 ligase and proteasomal destruction. The canonical IKKs also switch on the protein kinase Tpl2 by phosphorylating its inhibitory p105/NF- κ B1 component. Similarly, TAK1 not only initiates activation of the canonical IKKs but is also required to activate c-Jun N-terminal kinase (JNK) and p38 α mitogen-activated protein kinase (MAPK) via the TLR–MyD88 signaling pathway. The canonical IKKs and MAPKs then catalyze many further phosphorylation events that control the transcription, translation, processing, and secretion of inflammatory mediators (Sato et al., 2005; Shim et al., 2005).

Interestingly, the polyubiquitin-binding domain in NEMO, originally termed A20-binding inhibitor of NF- κ B (ABIN) homology domain 2 (AHD2; Heyninck et al., 2003), but later renamed the ubiquitin-binding domain in ABIN and NEMO (UBAN; Wagner et al., 2008), is found in four other human proteins, termed NRP (NEMO-related protein, also called optineurin), ABIN1, ABIN2, and ABIN3. The ABINs are so named because they were originally identified in a yeast two-hybrid screen using the protein deubiquitylase A20 as bait and because they were found to inhibit NF- κ B-dependent gene transcription when overexpressed in cells (Heyninck et al., 1999).

Recently, ABIN1 knockout mice were generated and characterized (Oshima et al., 2009). These mice were found at normal Mendelian ratios up to embryonic day (E) 18.5, but the embryos were smaller and more anemic than WT embryos and died during late embryogenesis from fetal liver apoptosis and hypoplasia. Embryonic fibroblasts isolated from the ABIN1^{-/-} mice were hypersensitive to TNF-induced programmed cell death and the lethality could be rescued by crossing to mice that did not express the TNFR1 receptor (Oshima et al., 2009).

To understand the physiological role of the polyubiquitin-binding function of ABIN1, we generated knockin mice that express the ABIN1[D485N] mutant instead of the WT protein, a mutation which is equivalent to the polyubiquitin binding-defective NEMO[D311N] mutant described already. Unexpectedly, these knockin mice had a quite different phenotype from the ABIN1^{-/-} mice. They were born at normal Mendelian frequencies and the adults were of normal size and weight. However, they then developed a lupus-like autoimmune disease, which could be prevented by crossing to MyD88-deficient mice. These and other results presented in this paper demonstrate that the interaction of ABIN1 with polyubiquitin chains limits the strength of signaling downstream of TLR–MyD88 and that this is critical to prevent autoimmunity.

RESULTS

Interaction of ABIN1 with polyubiquitin chains in vitro and generation of ABIN1[D485N] knockin mice

The mutation of Asp311 of NEMO to Asn prevents it not only from binding to K63-pUb chains (Ea et al., 2006; Wu et al., 2006)

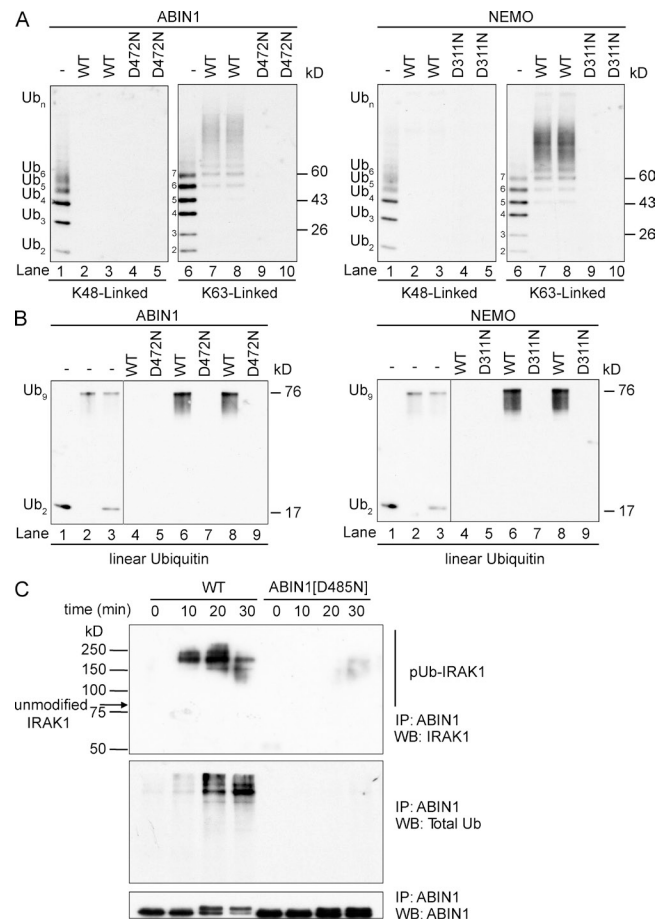


Figure 1. Binding to Lys63-linked or linear polyubiquitin chains is disrupted by a point mutation in the UBAN of ABIN1 or NEMO.

(A and B) The binding of WT and mutant human ABIN1 and NEMO to polyubiquitin chains is described in Materials and methods. Polyubiquitin chains captured by the immobilized proteins were released by denaturation in 1% (wt/vol) SDS, subjected to SDS-PAGE and immunoblotted with an anti-ubiquitin antibody (Dako). (A) Lanes 1 and 6 show, respectively, the K48-linked and K63-linked polyubiquitin preparations used in the experiment. The binding of K48-linked (lanes 2 and 3) and K63-linked (lanes 7 and 8) polyubiquitin chains to WT ABIN1 (left) or NEMO (right) and to the ABIN1[D472N] and NEMO[D311N] mutants (lanes 4, 5, 9, and 10, left and right) is shown. Similar results were obtained in two different experiments. (B) As in A, except that binding to linear polyubiquitin oligomers was studied. Lanes 1–3 show the di-ubiquitin and nona-ubiquitin preparations used in the experiment. Lane 4 shows the lack of binding to di-ubiquitin, lane 6 the binding to nona-ubiquitin, and lane 8 the selective capture of nona-ubiquitin by ABIN1 and NEMO when presented with a mixture of nona-ubiquitin and di-ubiquitin, and lanes 5, 7, and 9 the lack of binding of ABIN1[D472N] and NEMO[D311N] to linear ubiquitin oligomers. Similar results were obtained in two different experiments. Gray lines indicate that intervening lanes were spliced out. (C) BMDM from ABIN1[D485N] and WT mice were stimulated with 100 ng/ml LPS for the times indicated. ABIN1 was immunoprecipitated from the cell extracts and immunoblotted with anti-IRAK1 (top), anti-ubiquitin (middle), and anti-ABIN1 (bottom) antibodies. Similar results were obtained in two different experiments.

but also from binding to linear polyubiquitin chains (Rahighi et al., 2009). Linear polyubiquitin chains are thought to be generated by the LUBAC E3-ligase (Kirisako et al., 2006) and to

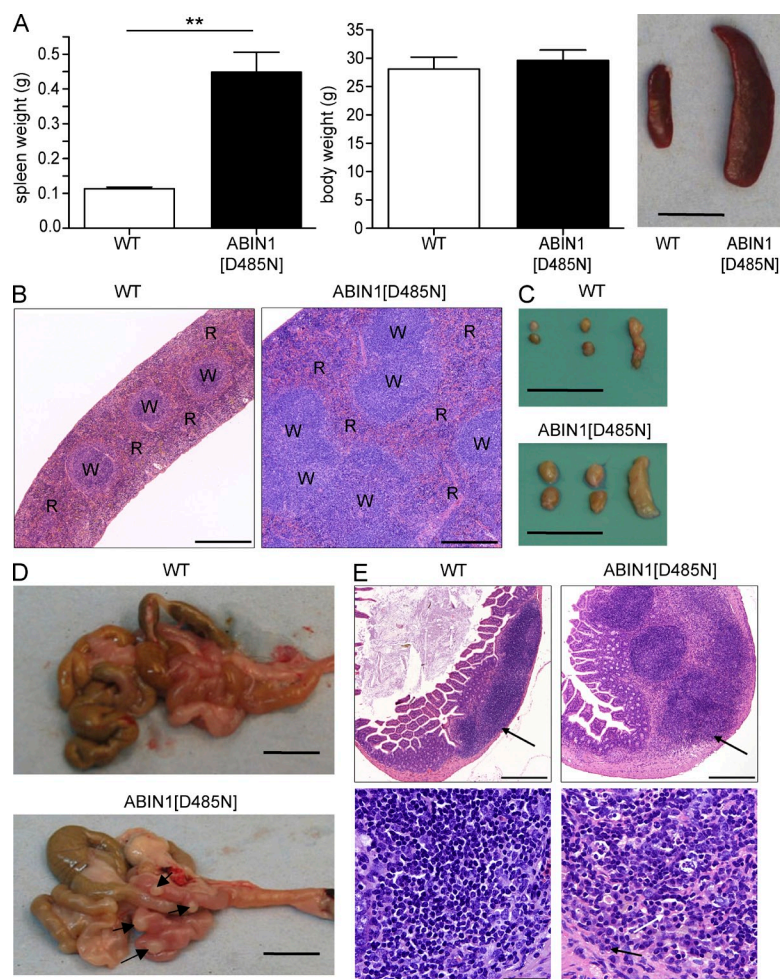


Figure 2. Spontaneous development of defects in multiple immune organs in ABIN1[D485N] mice.

(A) Mean spleen weight (left) and body weight (middle) of WT and ABIN1[D485N] knockin mice with a typically enlarged spleen in 4-mo-old mutant mice (right). Bar, 1 cm. (B) Representative photomicrograph of hematoxylin and eosin-stained spleen sections from WT and ABIN1[D485N] mice. The red (R) and white (W) pulp are indicated. Bars, 0.05 mm. (C) Axillary, inguinal, and mesenteric LNs of 5-mo-old ABIN1[D485N] mice compared with WT mice. Bars, 1 cm. (D) Gut-associated lymphoid tissue (arrows) of the small intestine wall of ABIN1[D485N] (bottom) and WT (top) mice. Bars, 1 cm. (E) Hematoxylin and eosin-stained sections of Peyer's patches (PP) in WT and ABIN1[D485N] mice. In the low-power view (top; bars, 0.5 mm), the arrows indicate Peyer's patches in ABIN1[D485N] mice compared with WT mice. In the high-power view (bottom; bar, 0.05 mm), there are Peyer's patches showing plasma cells (white arrows) and neutrophils (black arrow) in the ABIN1[D485N] mice. All mice used were 16–20 wk old. Data are representative of at least 12 mice (A–C) and 6 mice (D and E) of each genotype. Error bars show the mean \pm SEM. **, $P < 0.005$ (two-tailed Student's *t* test).

play an important role in activation of NF- κ B by TNF (Haas et al., 2009; Tokunaga et al., 2009). Before making a knockin mouse expressing a polyubiquitin-binding defective mutant of ABIN1, we therefore investigated whether the mutation to Asn of Asp472, the residue equivalent to Asp311 of NEMO, also prevented binding of human ABIN1 to polyubiquitin. When presented with a mixture of small ubiquitin oligomers linked via Lys63, ABIN1, like NEMO, preferentially captured the largest polyubiquitin chains in the preparation but did not bind detectably to K48-linked ubiquitin oligomers under the conditions tested (Fig. 1 A). ABIN1, like NEMO, also captured a linear ubiquitin oligomer consisting of nine ubiquitins but did not capture linear di-ubiquitin in our assay (Fig. 1 B). The ABIN1[D472N] mutant, like the NEMO[D311N] mutant, did not bind to either K63-linked (Fig. 1 A) or linear (Fig. 1 B) polyubiquitin chains. We therefore generated a knockin mouse in which WT ABIN1 was replaced by the ABIN1[D485N] mutant, which is equivalent to the ABIN1[D472N] mutant of human ABIN1 (Fig. S1, A and B).

The ABIN1[D485N] mutant was expressed at similar levels to WT ABIN1 in BM-derived macrophages (BMDMs), B cells, and T cells (Fig. S1, C–E). To check that the mouse

ABIN1[D485N] mutant was unable to bind to polyubiquitin chains *in vivo*, we immunoprecipitated the endogenous ABIN1 from BMDM extracts, followed by immunoblotting with anti-IRAK1 (to detect polyubiquitylated-IRAK1) and anti-ubiquitin. These experiments showed that stimulation with LPS induced the binding of ABIN1 to polyubiquitylated IRAK1 (Windheim et al., 2008) but not to unmodified IRAK1. In contrast, the ABIN1[D485N] mutant did not capture polyubiquitylated IRAK1 (Fig. 1 C).

Gross analysis of ABIN1[D485N] knockin mice

The ABIN1[D485N] mice were the same size and weight as WT littermates (Fig. 2 A) and were born at the expected Mendelian frequencies (not depicted). However, examination of their internal organs at 2–3 mo of age revealed enlarged spleens which, by 4 mo, were four to five times the weight of those from WT mice (Fig. 2 A). Both the white pulp and the red pulp were greatly enlarged in the spleen, although the splenic architecture was maintained (Fig. 2 B).

ABIN1[D485N] knockin mice had significantly enlarged LNs (Fig. 2 C) and 60–70% of the knockin mice had large nodule-like structures on the intestinal wall, which were identified as Peyer's Patches (Fig. 2, D and E). The size and number of these nodules varied between animals and resulted from plasmacytosis and infiltration of neutrophils (Fig. 2 E). Although young ABIN1[D485N] mice appeared to be superficially healthy, by 20 wk they all developed signs of severe autoimmunity, resulting in the majority of the knockin mice being terminated by 6 mo of age. This phenotype was exacerbated in the female mice during pregnancy.

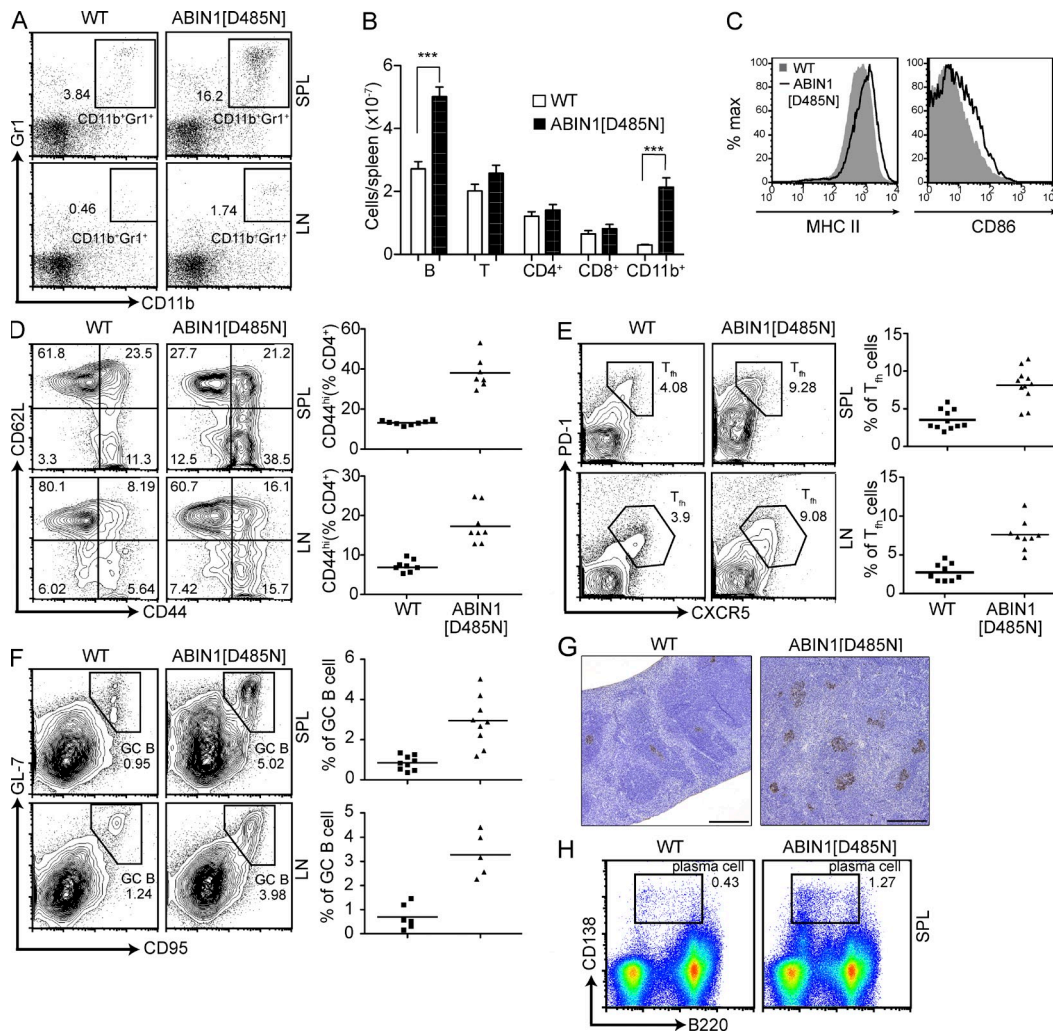


Figure 3. Defects in immune cells with spontaneous germinal center formation in ABIN1[D485N] mice. (A–F and H) Flow cytometric profiles of spleen (SPL) and LNs. Profiles were gated on: lymphocytes by FSC/SSC (C–F and H); live cells (A); TCR- β^+ CD4 $^+$ (D and E), and B220 $^+$ (C and F). The numbers within figures indicate the percentages of different cells. GC B, germinal center B cell. (A) Flow cytometric dot plots of spleen (top) and LN (bottom) showing frequencies of the CD11b $^+$ Gr1 $^+$ (macrophages and granulocytes) population in ABIN1[D485N] and WT mice. (B) Total cell numbers in spleens of ABIN1[D485N] mice compared with WT. Error bars show the mean \pm SEM. ***, $P < 0.001$ (two-tailed Student's t test). (C) Expression of B cell activation markers from WT (shaded area) and ABIN1[D485N] (black line). (D–F) Contour plots (left) and graphical analysis (right) showing percentages of cell populations in spleen (top) and LN (bottom). Each symbol represents one mouse and the horizontal bars show the mean of the values obtained. (D) Activated (CD4 $^+$ CD44 $^{\text{hi}}$ CD62L $^{\text{lo}}$) and naive (CD4 $^+$ CD62L $^{\text{hi}}$) T cells. (E) T $_{\text{H}}$ cells (CD4 $^+$ CXCR5 $^+$ PD-1 $^{\text{hi}}$). (F) Germinal center B cells (B220 $^+$ GL-7 $^+$ CD95 $^+$). (G) Immunohistochemistry of spleens from 16-wk-old mice with germinal centers (brown) stained with peanut agglutinin (PNA). Bars, 0.5 mm. (H) Expression of CD138 and B220 in spleen showing plasma cells in ABIN1[D485N] mice and WT mice. All mice analyzed were 12–16 wk old, and data are representative of at least three independent experiments with three to four mice of each genotype (A–F and H) or single experiment with six mice per genotype (G).

Defects in immune cells with spontaneous germinal center formation in the ABIN1[D485N] knockin mice

To investigate immunological changes in the mice, we performed flow cytometry analyses of various lymphoid organs. Analysis of splenic and LN cells revealed more B cells and granulocytes (CD11b $^+$ Gr1 $^+$) in the ABIN1[D485N] mice compared with WT mice (Fig. 3, A and B; and Fig. S2 A). The expression of MHCII and CD86 receptors on B cells was also increased in the spleen (Fig. 3 C) and LNs (not depicted) of the ABIN1[D485N] mice, indicating that the B cells were activated. However, the development of B cells in the BM and

the proportions of different B cell populations in the spleen, LNs, and peritoneal cavity of the ABIN1[D485N] mice did not differ significantly from those in the WT mice (Figs. S2, B–E). We also found that the ABIN1[D485N] knockin mice had four to five times the normal level of monocytes in the blood (unpublished data).

T cell development in the thymus was normal (Fig. S2 F). In contrast, analysis of the splenic and LN T cell populations demonstrated an increased proportion of activated effector T cells (CD62L $^{\text{lo}}$ and CD44 $^{\text{hi}}$) and a reduced proportion of naive T cells (CD62L $^{\text{hi}}$) compared with age-matched controls (Fig. 3 D).

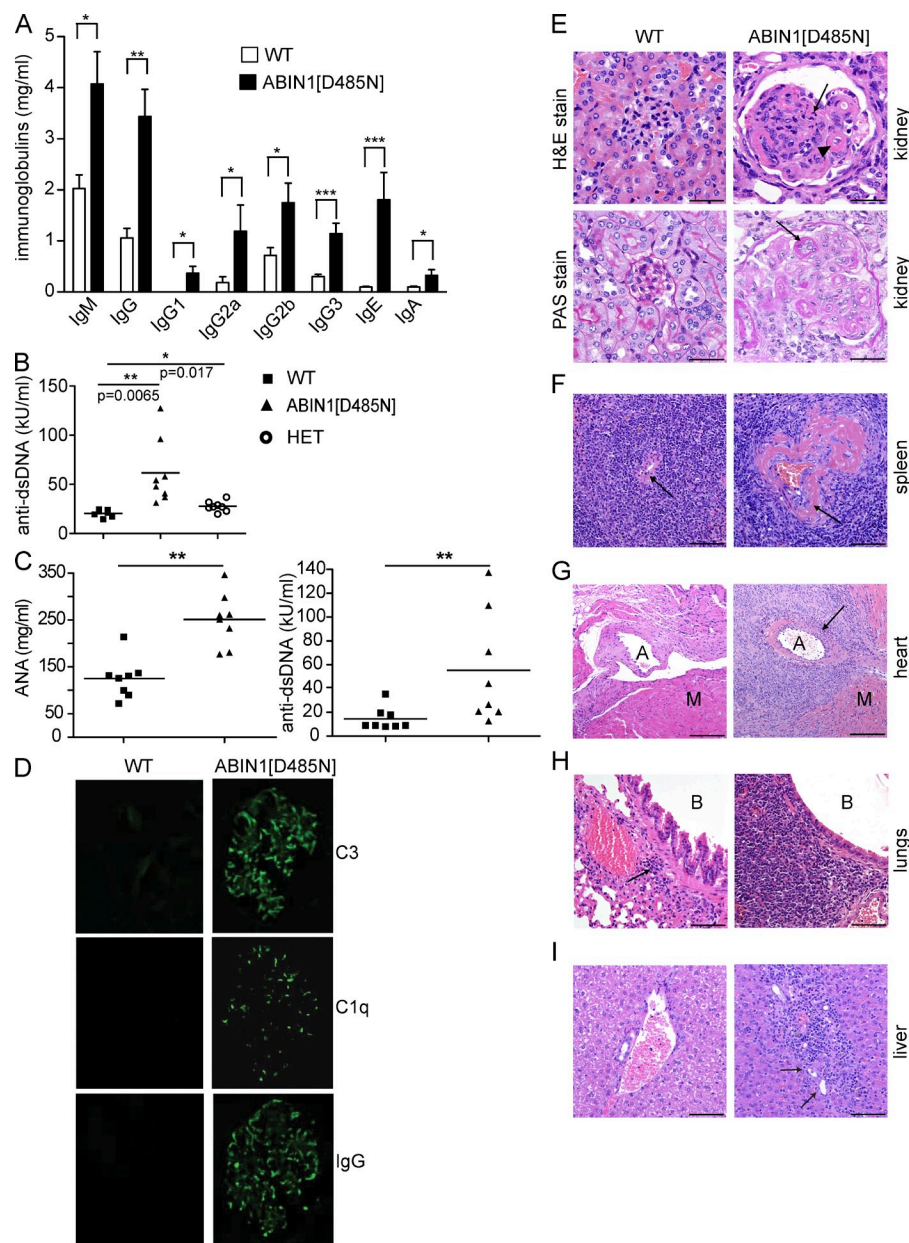


Figure 4. Autoimmune phenotypes in ABIN1[D485N] mice. Values were compared by the Mann-Whitney U test. *, $P \leq 0.05$; **, $P \leq 0.005$; ***, $P \leq 0.0005$. (A) Serum levels of immunoglobulin isotypes quantitated by ELISA in WT and ABIN1[D485N] mice. Error bars represent mean \pm SEM. (B) Level of anti-dsDNA antibodies in serum of 16-wk-old WT, ABIN1[D485N], and heterozygous (HET) mice measured by ELISA. (C) Total antinuclear antibodies (ANA; left) and anti-dsDNA antibodies (right) in the serum of 22-wk-old WT and ABIN1[D485N] mice were measured by ELISA. (B and C) Each symbol represents one mouse and the horizontal bars show the mean of the values obtained. (D) Kidney sections stained with fluorescein isothiocyanate-labeled anti-mouse C3, C1q, and IgG. (E) Kidney sections stained with hematoxylin and eosin (top) or PAS (bottom). In the top panel, the arrowhead shows glomerulonephritis with capillary loop thickening by eosinophilic material and the black arrow shows infiltration of mesangium by neutrophils. In the bottom panel, the arrow shows glomerulonephritis, with capillary wall thickening by PAS-positive staining. (F–I) Hematoxylin and eosin-stained sections of spleen, heart, lungs, and liver. (F) Spleen. The arrow indicates the WT (left) or congested splenic artery in ABIN1[D485N] mice (right) by eosinophilic material. Bars, 0.1 mm. (G) Heart. The arrow indicates infiltration of neutrophils and macrophages around arterial wall (A) in ABIN1[D485N] mice. M, myocardium. Bars, 0.2 mm. (H) Lungs. The arrows show plasma cells in the WT and ABIN1[D485N] mice. B, bronchus. Bars, 0.1 mm. (I) Liver, the portal tracts are shown by arrows. Bars, 0.1 mm. The data are from a single experiment with 7–9 (A–C) or 6–12 (D–I) mice per genotype.

However, the proportion of CD4⁺ and CD8⁺ T cells in the spleen was normal (Fig. S2 G).

It has been reported that an increased number of follicular helper T cell (T_{fh} cell) is associated with autoimmunity, and we therefore studied whether T_{fh} cell number was altered in the ABIN1[D485N] mice. These experiments revealed that the proportion of T_{fh} cells (CD4⁺ PD1^{hi} and CXCR5⁺) in the spleen and LN was greatly increased (Fig. 3 E), as were the number of germinal center B cells (B220⁺ CD95⁺ and GL7⁺; Fig. 3 F). Consistent with more germinal center B cells, there was increased formation of germinal centers in the spleens of ABIN1[D485N] mice (Fig. 3 G). There was also an increase in the proportion of extrafollicular plasma cells in the spleen of ABIN1[D485N] mice (Fig. 3 H).

Elevated levels of immunoglobulins and autoantibodies in the serum of ABIN1[D485N] mice

The hyperplasia of T_{fh} cells and germinal center B cells in the spleen and LN led us to investigate the serum immunoglobulin levels. A variety of immunoglobulin isotypes were elevated in the ABIN1[D485N] knockin mice compared with age-matched WT mice, which included both T cell–dependent and T cell–independent immunoglobulins. In particular, the levels of pathogenic immunoglobulins were increased significantly after 20 wk (Fig. 4 A). The circulating levels of antinuclear antibodies and antibodies against double-stranded (ds) DNA were also increased significantly after 16 wk (Fig. 4 B) or 20 wk (Fig. 4 C) in the ABIN1[D485N] knockin mice, demonstrating that some of the antibodies in the knockin mice were being

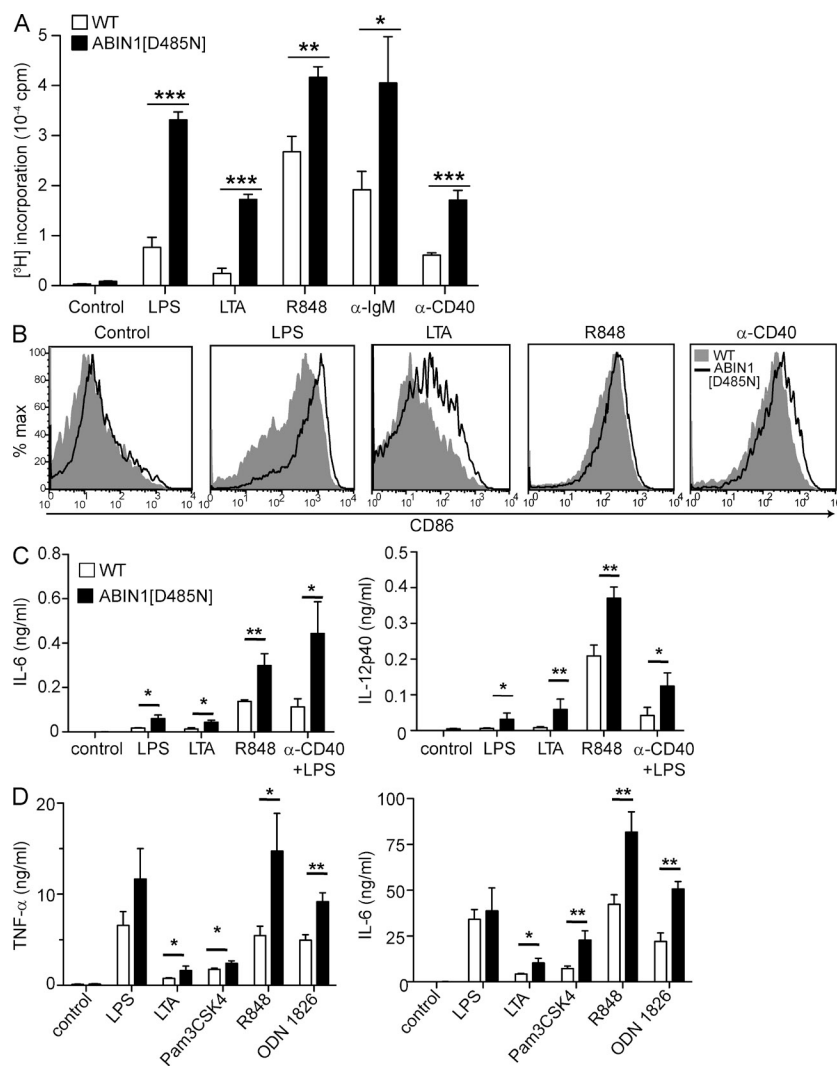


Figure 5. Enhanced activation of B cells and myeloid cells in ABIN1[D485N] mice. (A) Naive purified splenic B cells from WT and ABIN1[D485N] mice were stimulated with 200 ng/ml LPS, 10 μg/ml LTA, 200 ng/ml of the TLR7 agonist R848, 10 μg/ml α-IgM, or 1 μg/ml α-CD40 for 72 h or left unstimulated (control) before pulsing for a further 16 h with [³H]thymidine (0.5 μCi/well). [³H]thymidine incorporation into DNA was measured by harvesting and washing the cells followed by measurement of radioactivity incorporated. (B) Flow cytometric analysis of surface expression of the activation marker CD86 after stimulation of purified B cells with the agonists indicated. The filled histograms show results for WT cells and the empty histograms show the ABIN1[D485N] cells. (C) IL-6 and IL-12p40 secreted into the culture medium of B cells 48 h after exposure to the agonists indicated. (D) IL-6 and TNF secreted into the culture medium of BMDC 24 h after exposure to 100 ng/ml LPS, 2 μg/ml LTA, 1 μg/ml Pam3CSK4, 1 μg/ml R848, or 1 μM of the TLR9 agonist ODN 1826. Data are representative of five (A) or three (B–D) independent experiments with three to four mice of each genotype analyzed together. Error bars represent mean ± SD. *, $P \leq 0.05$; **, $P \geq 0.005$; ***, $P \leq 0.005$ (two-tailed Student's *t* test).

produced against self-cellular components, a feature of autoimmune disease. The heterozygous ABIN1[D485N]^{+/-} mice, which did not develop any pathological abnormalities, only had marginally elevated levels of anti-dsDNA (Fig. 4 B).

High levels of pathogenic immunoglobulins in the serum are known to be deposited in the kidney and the blood vessels, initiating an inflammatory reaction in these organs. We found that there was immune complex deposition in the kidney of the ABIN1[D485N] mice, leading to activation of the complement pathway (Fig. 4 D) and the development of severe renal disease at 20–24 wk of age. Histologically, this was revealed by severe generalized global membranoproliferative glomerulonephritis of the kidney with infiltration of neutrophils and plasma cells (Fig. 4 E, top). There was also thickening of glomerular capillary loops and Bowman's capsule basement membrane regions by periodic acid-Schiff (PAS)-positive material (Fig. 4 E, bottom).

Vascular lesions were noted at the same age in multiple sites, including splenic arterioles (Fig. 4 F) and heart-base arteries (Fig. 4 G), with occasional involvement of Peyer's Patch arterioles

and peripancreatic arteries (not depicted). The normal architecture of the walls of affected splenic arterioles was largely replaced by fibrinous material with scattered nuclear debris and mononuclear inflammatory cells (fibrinoid necrosis), and by extravascular leakage (Fig. 4 F). Similar changes were noted in heart-base arteries but with more severe inflammatory cell infiltrates, including neutrophils, macrophages, and reactive fibroblasts, which not only segmentally obliterated arterial wall architecture but also extended into the adjacent atrial myocardium (Fig. 4 G). Similarly, in lung tissue of most mice, the peribronchial lymphoid tissue was variably expanded by increased numbers of plasma cells (Fig. 4 H). Other histological lesions included expansion of hepatic portal tracts by variably (but often markedly) increased numbers of hematopoietic cells, lymphocytes, plasma cells, macrophages, and neutrophils with bridging fibrosis and biliary hyperplasia (Fig. 4 I).

The combination of lesions may explain why all the ABIN1[D485N] mice developed severe symptoms of autoimmune disease, requiring them to be culled within 6 mo, if they had not died already. In contrast, no WT control mice had died at this age.

Enhanced proliferation, cytokine production, and activation of signaling pathways in B cells and myeloid cells, but not T cells, from ABIN1[D485N] knockin mice

To understand why abnormal levels of immunoglobulins were present in the serum, we studied B cell function in

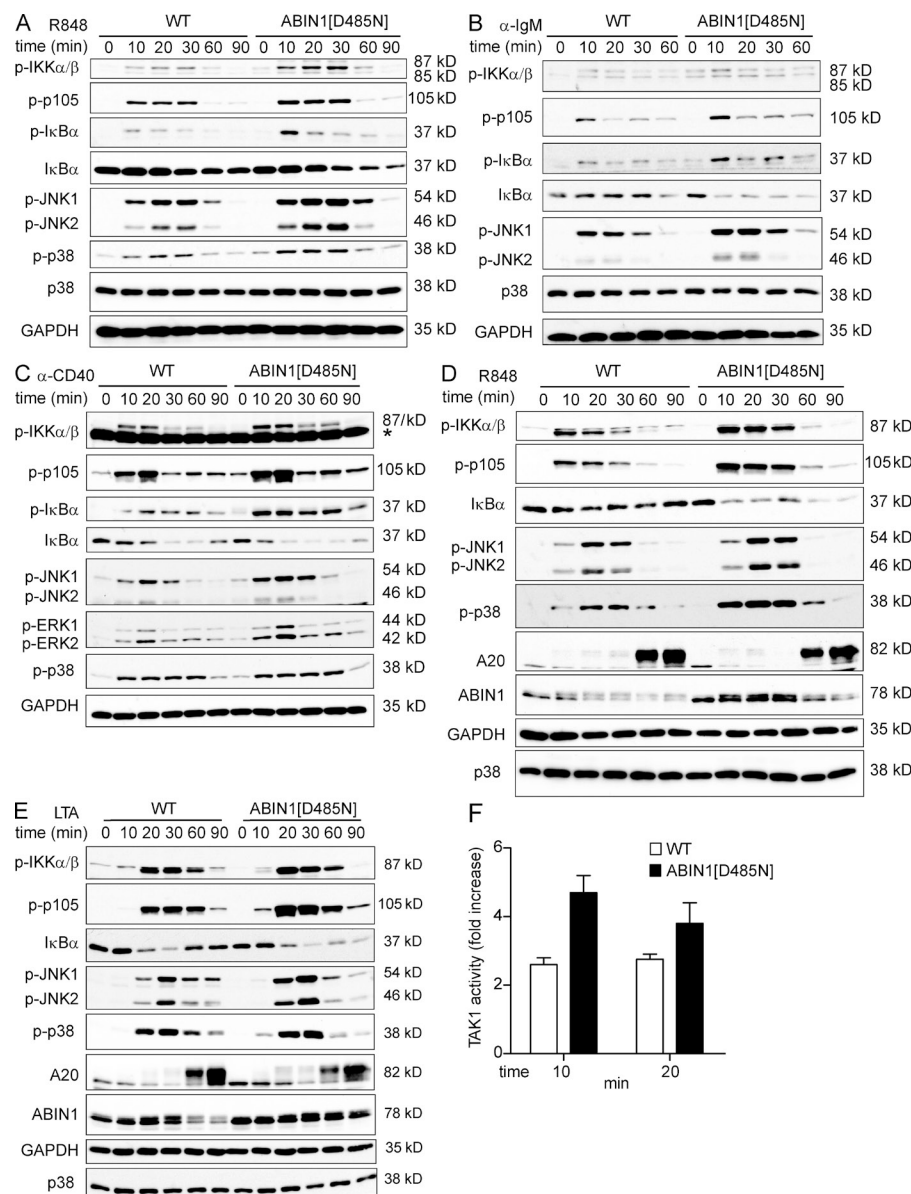


Figure 6. Activation of signaling pathways in B cells and BMDC from WT and ABIN1[D485N] mice. (A–C) B cells from WT and ABIN1[D485N] mice were stimulated with 0.5 μ g/ml of the TLR7 agonist R848 (A), 10 μ g/ml α -IgM (B), or 10 μ g/ml α -CD40 (C) for the times indicated, and cell lysates were probed with the antibodies indicated. *, nonspecific band. Antibodies that recognize GAPDH and p38 MAPK served as loading controls. The α -phospho (p)-IKK- α/β antibody in C–E (Ser176/180, antibody 16A6; Cell Signaling Technologies) differed from that used in A and B (Ser180/181; Cell Signaling Technologies). (D and E) BMDC from WT and ABIN1[D485N] mice were stimulated with 0.25 μ g/ml of the TLR7 agonist R848 (D) or 2 μ g/ml of the TLR2/6 agonist LTA (E) for the times indicated, and cell lysates were probed with the antibodies indicated. (A–E) The data are representative of two to four independent experiments. (F) BMDC were stimulated with 0.5 μ g/ml R848 for the times indicated and lysed, and TAK1 was immunoprecipitated with α -TAK1 and assayed as described in Materials and methods. The activity is plotted as fold increase compared with that measured in the lysates from cells not been stimulated with R848. The results are average data from three different experiments, each with BMDC from different mice, with each sample being assayed in duplicate. Error bars represent mean \pm SEM.

the mutant mice because these cells are major producers of immunoglobulins in vivo. Using purified naive B cells from the spleens of 5–6-wk-old mice before the onset of splenomegaly, we found that the TLR4 agonist LPS, the TLR2/6 agonist lipoteichoic acid (LTA), and the TLR7 agonist R848, as well as anti-IgM and anti-CD40, stimulated B cell proliferation more strongly in the ABIN1[D485N] mice than in the WT mice (Fig. 5 A). In contrast, the B cells from WT and ABIN1[D485N] mice proliferated similarly in response to the TLR9 ligand ODN1826 (unpublished data). The increased proliferation of B cells in response to anti-IgM and anti-CD40 was not explained by differences in the expression of these receptors, which were similar in ABIN1[D485N] and WT mice (unpublished data). The stimulation of B cells with either TLR agonists or anti-CD40 also increased the expression of the co-stimulatory molecule CD86, which was

more marked in the ABIN1[D485N] knockin cells (Fig. 5 B), and this might contribute to the increased activation of T cells via interaction with the CD28 receptor on T cells. In contrast, stimulation of purified CD4⁺ T cells with anti-CD3, alone or in combination with either CD28 or IL-2, resulted in similar proliferation rates in WT and ABIN1[D485N] knockin cells (Fig. S3 A), and the production of T cell cytokines tested was similar in different genotypes (Fig. S3 B). There was also no effect of the knockin mutation on the expression of inducible co-stimulator (ICOS) or the T cell activation markers CD25 or CD69 after TCR stimulation (unpublished data), again indicating that the increased proportion of activated T cells and T_h cells may not be explained by a T cell-intrinsic defect. Collectively, these results indicated that the T cell phenotypes observed in the ABIN1[D485N] mice may not have been caused by an intrinsic alteration in T cell receptor signaling. It has been well documented that regulatory T cells (T reg cells) play an important role in autoimmunity by limiting the activation of T cells, and that a decreased T reg cell number can cause autoimmunity. However, the proportion of T reg cells in the

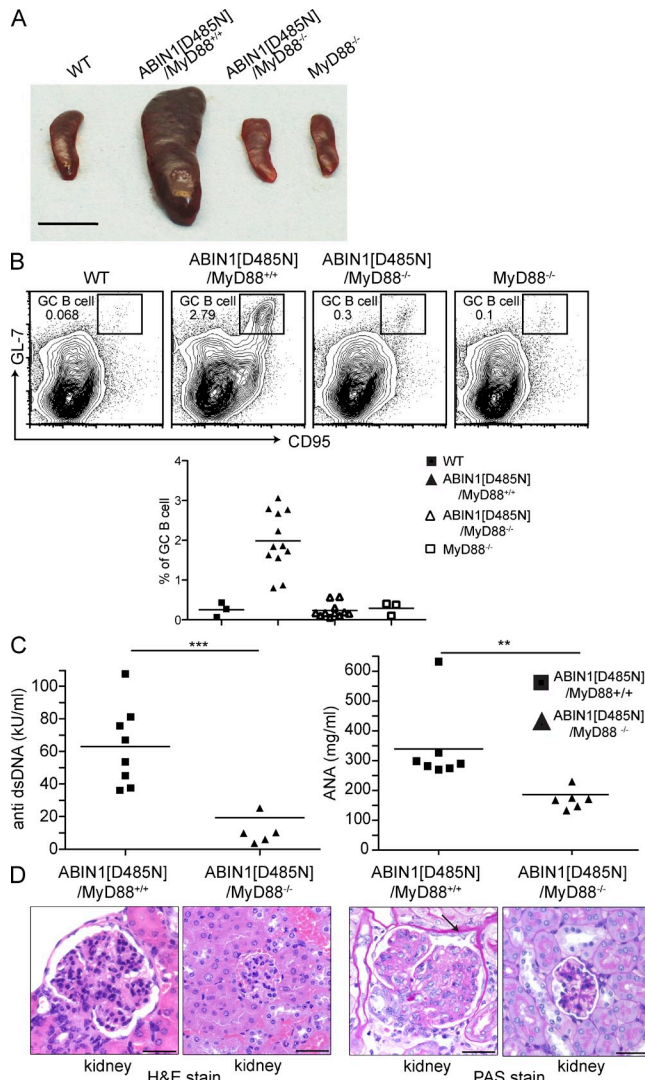


Figure 7. Comparison of the phenotypes of WT, ABIN1[D485N], ABIN1[D485N]/MyD88^{-/-}, and MyD88^{-/-} mice. (A) Spleen sizes of WT, ABIN1[D485N]xMyD88^{+/+}, ABIN1[D485N]xMyD88^{-/-}, and MyD88^{-/-} mice. Bar, 1 cm. A typical result from many mice analyzed is shown. (B) Flow cytometric analysis was performed as in Fig 2, and a representative set of contour plots is presented (top) showing the proportion of germinal center (GC) B cells (B220⁺ GL-7⁺ CD95⁺) in WT, ABIN1[D485N]xMyD88^{+/+}, ABIN1[D485N]xMyD88^{-/-}, and MyD88^{-/-} mice. Similar results were obtained in three independent experiments. On the bottom, the percentage of GC B cells is shown for each WT type (filled squares), ABIN1[D485N]xMyD88^{+/+} (filled triangles), ABIN1[D485N]xMyD88^{-/-} (open triangles), and MyD88^{-/-} (open squares) mouse examined. Each symbol represents an individual mouse and the horizontal bar shows the mean of the values obtained. (C) Anti-dsDNA antibodies and ANA antibodies in ABIN1[D485N]xMyD88^{+/+} mice (filled squares) and ABIN1[D485N]xMyD88^{-/-} mice (filled triangles). Data are shown for a single experiment with six to eight mice of each genotype. ***, $P < 0.005$; **, $P > 0.005$ (Mann-Whitney U test). Each symbol represents an individual mouse and the horizontal bar shows the mean of the values obtained. (D) Hematoxylin and eosin (H&E) staining (first two panels) and PAS staining (third and fourth panels) of kidney sections from ABIN1[D485N]xMyD88^{+/+} and ABIN1[D485N]xMyD88^{-/-}. Bars, 0.05 mm.

ABIN1[D485N] mice was only slightly higher than that in WT mice (Fig. S3 C).

The stimulation of B cells with LPS alone, or the combination of LPS with anti-CD40, also induced higher levels of IL-6 and IL-12p40 secretion in the ABIN1[D485N] mice compared with WT mice. Similar results were found with LTA and R848 (Fig. 5 C). Moreover, TLR stimulation of other immune cells of myeloid origin, such as BM-derived DCs (BMDCs), also increased production of IL-6 and other proinflammatory cytokines, such as TNF, more markedly in the cells from the ABIN1[D485N] mice (Fig. 5 D).

The results described in the previous paragraph suggested that signaling events required for the production of cytokines by B cells and myeloid cells were being switched on more strongly in the ABIN1[D485N] mice compared with WT, and they led us to examine the activation of these pathways. Stimulation of naive splenic B cells with the TLR7 ligand R848 (Fig. 6 A), the TLR4 ligand LPS (Fig. S4 A), the B cell receptor (BCR) ligand (anti-IgM; Fig. 6 B), or the CD40 agonist (anti-CD40; Fig. 6 C) caused enhanced phosphorylation (activation) of the canonical IKKs (IKK- α/β) and the phosphorylation of their substrates p105/NF- κ B1 and I κ B α in the ABIN1[D485N] mice compared with WT mice, and, consistent with enhanced phosphorylation (activation) of the MAPKs JNK1/2 and p38 α MAPK. Enhanced activation of the canonical IKKs and MAPKs was also observed in BMDC and BMDM from ABIN1[D485N] mice compared with WT mice after stimulation with LTA or the TLR7 agonist R848 (Fig. 6, D and E; and Fig. S4, B and C).

The finding that activation of MAPKs, as well as the canonical IKK complex, was enhanced in immune cells from the ABIN1[D485N] mice after TLR stimulation indicated that ABIN1 must be exerting its effect by suppressing the activation of a more upstream component of the pathway. This led us to examine the activation of TAK1 and to show that it is also enhanced in BMDC from the knockin mice compared with WT mice (Fig. 6 F).

Enhanced activation of the nucleotide oligomerization domain (NOD) 1–NOD2 signaling pathway

The cytoplasmic proteins NOD1 and NOD2 detect peptidoglycan components from intracellular bacteria that have evaded the TLR defense system (Inohara et al., 2005). The activation of these receptors induces their interaction with the protein kinase RIP2, leading to the activation of NF- κ B, MAPKs, and inflammatory mediators by a pathway that appears to intersect with the TLR signaling pathway at the level of TAK1 (Windheim et al., 2007). We found that the peptidoglycan-stimulated activation of NOD1 (Fig. S4 D) and NOD2

The arrow shows PAS-positive material. Three or four mice of each genotype were analyzed and a representative result is shown.

(not depicted) induced a far stronger activation of IKK- α/β and MAPKs in BMDM from the ABIN1[D485N] mice than WT mice.

The absence of MyD88, but not RIP2, suppresses the autoimmune phenotype of ABIN1[D485N] mice

The results presented in the previous section suggested that enhanced activation of one or more cell signaling pathways might underlie or contribute to the autoimmune phenotype of the ABIN1[D485N] mice. To investigate the importance of the TLR-MyD88-dependent and NOD1/2-RIP2 signaling pathways, we crossed the ABIN1[D485N] mice with mice that do not express the adaptor MyD88 (required for TLR-MyD88 signaling) or with mice that do not express RIP2. The ABIN1[D485N] \times RIP2 $^{-/-}$ mice still displayed all the gross phenotypes of the ABIN1[D485N] mice (splenomegaly, lymphadenopathy, and intestinal nodules) and flow cytometry analysis did not show rescue of any immune phenotype (unpublished data). The ABIN1[D485N] \times MyD88 $^{-/-}$ mice, however, did not develop splenomegaly (Fig. 7 A), enlarged LNs, and intestinal nodules (not depicted). They had greatly reduced numbers of germinal center B cells in the spleen (Fig. 7 B), and serum levels of anti-dsDNA, antinuclear antibodies (Fig. 7 C), and different immunoglobulins (not depicted) were also greatly reduced in the ABIN1[D485N] \times MyD88 $^{-/-}$ mice. Moreover, no glomerulonephritis was observed in the kidneys of the ABIN1[D485N] \times MyD88 $^{-/-}$ after 20–24 wk (Fig. 7 D). Interestingly, the increased number of activated T cells and T_H cells in the ABIN1[D485N] mice also returned to the level found in WT mice in the ABIN1[D485N] \times MyD88 $^{-/-}$ mice (Figs. S5, A and B).

CD40 is not thought to signal via MyD88 (He et al., 2010a), but using B cells from age-matched ABIN1[D485N] mice, MyD88 $^{-/-}$ mice, ABIN1[D485N]/MyD88 $^{-/-}$ mice, and WT mice, we found that the enhanced activation of the canonical IKKs and JNK observed in CD40-stimulated B cells from the ABIN1[D485N] mice was reduced in B cells from the ABIN1[D485N]/MyD88 $^{-/-}$ mice to the same level found in either WT mice or MyD88 $^{-/-}$ mice (unpublished data). This suggests that the over-reactivity of the ABIN1[D485N]-expressing B cells to CD40 depends on MyD88 signaling. This suggests that there may be cross talk between the CD40 and MyD88 signaling pathways, which would be interesting to investigate in future studies.

Generation of ABIN1[D478–606] mice

The way in which the targeting vector for the ABIN1[D485N] mice was designed allowed the targeted region to be removed by crossing to CRE deleter mice, which generated a form of ABIN1 in which residues 478–606 were deleted. This deletion did not cause the truncated protein to misfold and be degraded, and the ABIN1[Δ 478–606] mutant was actually expressed at higher levels than WT ABIN1 in BMDM (Fig. S6 A) and embryonic fibroblasts (not depicted). The ABIN1[Δ 478–606] mice were also born at near Mendelian frequencies and

had a similar phenotype to the ABIN1[D485N] mice (Fig. S6 B), although it was slightly more severe, in as much as the mice became moribund about a month earlier than the ABIN1[D485N] mice. As found in the ABIN1[D485N] mice, there was enhanced activation of TLR signaling pathways in BMDM from the ABIN1[Δ 478–606] mice (Fig. S6 A).

TNF-induced apoptosis in embryonic fibroblasts from ABIN1[D485N] mice

ABIN1 $^{-/-}$ mice were reported to be found at normal Mendelian ratios up to E18.5, but the embryos then died during late embryogenesis from fetal liver apoptosis and hypoplasia. Embryonic fibroblasts isolated from the ABIN1 $^{-/-}$ mice were hypersensitive to TNF-induced apoptosis, and the lethality could be rescued by crossing to mice that did not express the TNFR1 receptor (Oshima et al., 2009). The TNF-stimulated apoptosis could be restored to normal levels by reintroducing WT ABIN1 but not by reintroduction of the ABIN1[D485N] mutant. Consistent with these findings, we found that embryonic fibroblasts from the ABIN1[D485N] knockin mice also showed enhanced TNF-induced apoptosis (Fig. S7, C and D). The reason why the ABIN1[D485N] and the ABIN1[Δ 478–606] mice that we generated did not display embryonic lethality is unclear but could be the result of a difference in the background of the mice.

In contrast to the effect of TNF on apoptosis, the TNF-stimulated activation of NF- κ B was reported to be similar in embryonic fibroblasts from ABIN1 $^{-/-}$ mice and WT mice (Oshima et al., 2009). Consistent with this finding, we did not see enhanced activation of MAPKs or the canonical IKK complex in embryonic fibroblasts from the ABIN1[D485N] mice, although these signaling pathways were activated a little more strongly in IL-1-stimulated fibroblasts from the ABIN1[D485N] mice (Fig. S7).

DISCUSSION

In this paper, we demonstrate that replacing a single aspartate in the UBAN of ABIN1 (Asp485) by an asparaginyl residue, which suppresses the binding of ABIN1 to K63-pUb chains or linear pUb chains, causes autoimmunity in mice. Immune cells from the ABIN1[D485N] knockin mice showed enhanced activation of signaling pathways in response to TLR agonists that signal via MyD88, leading to increased B cell proliferation and enhanced production of IL-6 and IL-12p40 production by B cells and elevated IL-6 and TNF by myeloid cells. The critical role of TLR signaling pathways in driving autoimmunity was indicated by the finding that the phenotype was suppressed completely when the ABIN1[D485N] knockin mice were crossed to MyD88 $^{-/-}$ mice. These observations raised the question of how increased signaling via TLR-MyD88 pathways can lead to autoimmunity.

Autoimmunity probably results from the formation of many germinal centers that were present in the spleens of the ABIN1[D485N] mice and are responsible for antibody isotype switching and the production of pathogenic antibodies. As suggested by others (Vinuesa et al., 2005, 2009), the formation

of germinal centers may be triggered by the presence of abnormally high numbers of T_{fh} cells, which was a feature of the spleen and LNs of the ABIN1[D485N] knockin mice. An increase in the number of T_{fh} cells can result from the aberrant expression of ICOS molecules on T cells (Vinuesa et al., 2005) and be stimulated by IL-6 and IL-12 (Nurieva et al., 2008; Ma et al., 2009; Schmitt et al., 2009). We did not observe any changes in T cell receptor activation or increased production of ICOS by T cells in the ABIN1[D485N] mice compared with WT mice after TCR stimulation. It therefore seems more likely that increased IL-6 and IL-12 secretion in B cells and myeloid cells via the TLR-MyD88 pathway, coupled with increased expression of co-stimulatory molecules (CD80 and CD86) by antigen-presenting cells, underlies the increased number of T_{fh} cells in the mutant animals. Enhanced TLR signaling could, however, lead to germinal center formation in other ways. For example, the migration of B cells to form new germinal centers can be driven by stimulation of TLR4 (Hwang et al., 2009) or TLR7 (Bessa et al., 2010) *in vivo*, even in IL-21^{-/-} mice where T_{fh} cell function is defective. Another potentially important mechanism by which TLR-MyD88 signaling pathways contribute to autoimmunity is via the hyperactivation of T reg cells, leading to loss of their ability to suppress effector T cell responses (Pasare and Medzhitov, 2004; Peng et al., 2005; Suttmüller et al., 2007). In summary, our studies with the ABIN1[D485N] mice provide striking support for the concept that abnormally high TLR-MyD88 signaling can trigger autoimmunity (Marshak-Rothstein, 2006).

The increased production of interferon α in plasmacytoid DCs by TLR7 and/or TLR9 agonists is reported to be involved in the development of lupus-like autoimmunity (Banchereau and Pascual, 2006), raising the question of whether ABIN1 prevents autoimmunity by limiting TLR7/TLR9-stimulated interferon α production by pDC. However, we were unable to detect any increase in interferon α production by pDCs from ABIN1[D485N] mice compared with pDCs from WT mice in response to the TLR7 agonist poly(dU) or the TLR9 agonist ODN1826 (unpublished data).

An important unresolved question is the identity of the endogenous ligands that initiate activation of the TLR-MyD88 pathways in these animals *in vivo*. One possibility is that endogenous host RNA and/or DNA is able to activate TLR7 and TLR9 in the ABIN1[D485N] mice but not in WT mice. Alternatively, components of commensal bacteria may activate the TLR-MyD88 pathways resulting in autoimmunity, as observed in mice that do not express TANK (TRAF-associated NF- κ B activator), which also display enhanced activation of NF- κ B in response to ligands that signal via the TLR-MyD88 dependent pathway (Kawagoe et al., 2009). To investigate whether commensal bacteria were involved in the development of the phenotype, we fed the mice from birth with broad spectrum antibiotics, but this had no effect on the phenotype. The level of anti-dsDNA in the serum after 16 wk was 20.47 ± 3.69 kU/ml ($n = 8$) and 19.42 ± 8.19 kU/ml ($n = 9$), respectively, in control and antibiotic-fed WT mice, and rose to 61.54 ± 33.26 kU/ml ($n = 8$) and

78.55 ± 31.57 kU/ml ($n = 5$), respectively, in control and antibiotic-fed ABIN1[D485N] mice. Moreover, the antibiotic-fed ABIN1[D485N] mice had similar enlargement of the spleen and LNs. In contrast, the control IL-10^{-/-} mice, which were fed the same combination of antibiotics in parallel, were protected against the development of ulcerative colitis and anal prolapse, as expected.

How polyubiquitin binding to WT ABIN1 limits the strength of TLR-MyD88 signaling is a complex issue and a full molecular understanding will require further analysis. However, the studies we have performed in this paper indicate that ABIN1 exerts its inhibitory effects downstream of MyD88 but upstream of TAK1, explaining why the activation of JNK and p38 α MAPK, as well as the canonical IKKs, is enhanced in immune cells from the ABIN1[D485N] mice. Enhanced activation of TAK1 can also explain why the NOD1/2-RIP2 signaling pathway was activated more strongly in peptidoglycan-stimulated BMDM from ABIN1[D485N] mice and why B cells from the mutant mice proliferated more rapidly than B cells from the WT mice in response to BCR and CD40 agonists because TAK1 is known to be required for NOD1/2-RIP2 (Windheim et al., 2007), BCR, and CD40 signaling (Sato et al., 2005).

ABIN1 was originally identified as a protein that interacts with the deubiquitylase A20. Like ABIN1, A20 is known to function as a negative regulator of the innate immune system and mice with a conditional knockout of A20 in B cells develop autoimmunity (Boone et al., 2004; Tavares et al., 2010; Chu et al., 2011). Moreover, human polymorphisms in A20 predispose to autoimmune diseases (Plenge et al., 2007; Thomson et al., 2007; Nair et al., 2009). A priori, one might therefore have imagined that by binding to K63-pUb chains/proteins generated in response to TLR activation (see Introduction), ABIN1 may recruit A20 to its substrates, facilitating the A20-catalysed hydrolysis of K63-pUb chains/proteins and the inhibition of TLR-MyD88-dependent signaling. Cells expressing the polyubiquitin binding-defective ABIN1[D485N] mutant would be unable to perform this function, leading to increased levels of K63-pUb chains/proteins and enhanced recruitment and activation of the TAK1 complex. However, whether this is the way in which ABIN1 limits the strength of signaling is unclear for several reasons. First, the bacterially expressed A20 catalytic domain cleaves K48-pUb chains and not K63-pUb chains or linear polyubiquitin chains *in vitro* (Komander et al., 2009), although A20 may be able to hydrolyze K63-pUb chains when overexpressed in mammalian cells (Wertz et al., 2004), in which case there may be a mechanism for altering the specificity of A20 *in vivo*. Second, a truncated form of ABIN1, ABIN1[444–601], which does not interact with A20, inhibits TNF-stimulated NF- κ B-dependent gene transcription as effectively as WT ABIN1 in overexpression experiments (Heyninck et al., 2003). Third, the level of A20 is low in unstimulated cells and increases greatly after stimulation for 1 h with TLR agonists (Fig. 6, C and D), but the enhanced activation of signaling pathways in immune cells from the ABIN1[D485N] mice can be observed

after only 10–15 min (Fig. 6), demonstrating that this effect is independent of the induction of A20. Fourth, although the B cell–specific knockout of A20 leads to autoimmunity, the onset of the pathology seems to be delayed by several months compared with the ABIN1[D485N] mice (Tavares et al., 2010). Therefore, if the phenotype of the ABIN1[D485N] mice is driven only by alterations in B cell function, it would be difficult to explain this solely by the loss of ABIN1-dependent recruitment of A20 to its substrates.

ABIN1 binds linear polyubiquitin chains, as well as K63-polyubiquitin chains (Fig. 1), and LUBAC, an E3 ligase which produces linear polyubiquitin specifically in vitro, appears to participate in at least one MyD88-dependent signaling pathway because the IL-1-stimulated activation of the canonical IKK complex was reported to be impaired in MEFs deficient in HOIL-IL, a component of LUBAC (Tokunaga et al., 2009). Therefore, the possibility that ABIN1 restricts signaling to NF- κ B by binding to linear polyubiquitin chains as well as, or instead of, K63-pUb chains cannot be excluded at this stage. However, the activation of JNK by TNF was not inhibited in HOIL-IL^{-/-} MEFs, implying that LUBAC is not required for the activation of TAK1. Moreover, the TAB2 component of the TAK1 complex binds to K63-pUb tetramers >100-fold more strongly than to linear ubiquitin tetramers (Kanayama et al., 2004; Kulathu et al., 2009; Sato et al., 2009). WT ABIN1 might therefore compete with the polyubiquitin-binding components of the TAK1 complex (TAB2–TAB3) for binding to the same K63-pUb chains/proteins, limiting the extent of activation of TAK1. We also observed in the present study that the endogenous polyubiquitylated IRAK1 could be coimmunoprecipitated with WT ABIN1, but not with ABIN1[D485N], from the extracts of LPS-stimulated BMDM. Therefore, another possibility is that the interaction of WT ABIN1 with polyubiquitylated IRAK1 may hinder the ability of IRAK1 to interact with and activate TRAF6, reducing the TRAF6-mediated formation of K63-pUb chains and limiting the activation of TAK1. IRAK1 undergoes Lys63-linked polyubiquitylation in response to IL-1 (Windheim et al., 2008), but the possibility that it also undergoes linear polyubiquitylation has not been excluded.

Interestingly, while this study was in progress, human polymorphisms were identified in the gene encoding ABIN1 that predispose to lupus-like autoimmune diseases, psoriasis (Han et al., 2009; Nair et al., 2009), and vasculitis (He et al., 2010b). This suggests that ABIN1 also plays a key role in preventing autoimmunity in man. The ABIN1[D485N] mice may therefore be a good model for human autoimmune disease and could be used to assess the efficacy of drugs that target components of TLR–MyD88 signaling pathways. Drugs that increase the expression of ABIN1 could also have therapeutic value because the adenovirus-mediated delivery of ABIN1 to the lung epithelium has been reported to reduce allergen-induced eosinophil infiltration of the lungs in a mouse model of allergen-induced asthma (El Bakkouri et al., 2005).

MATERIALS AND METHODS

Expression and purification of ABIN1 and NEMO and binding to polyubiquitin. Human ABIN1 and ABIN1[D472N] were cloned and expressed as fusion proteins with glutathione *S*-transferase (GST) at the N terminus and a His₆ tag at the C terminus. The expressed proteins were purified on nickel-nitrilotriacetate agarose (QIAGEN) followed by chromatography on glutathione-Sepharose (GE Healthcare). Human NEMO and NEMO[D311N] were expressed as GST fusions and purified on glutathione-Sepharose. 8 μ g of these proteins were immobilized individually on a 10- μ l packed volume of glutathione-Sepharose and incubated for 1 h at 21°C with 2 μ g of K48-linked, K63-linked (Boston Biochem), or linear ubiquitin oligomers (Enzo Life Sciences) in 300 μ l 25 mM HEPES, pH 7.5, 1 mM EGTA, 0.5% (vol/vol) Triton X-100, and 2 mM MgCl₂ (Buffer A) plus 150 mM NaCl. The beads were washed five times with Buffer A plus 250 mM NaCl and once with Buffer A without Triton X-100.

Generation of ABIN1[D485N] knockin mice. The Asp485 to Asn knockin mutation was generated in exon 14 of the ABIN1 locus and, at the same time, LoxP sites were inserted in the introns adjacent to exons 14 and 16 by standard gene targeting methods (Fig. S1 A). The following primers were used for making the targeting vector (underlined regions indicate the presence of introduced restriction sites or LoxP sequences): 5' arm sense (5'-GAGCGGCGCCAGACCTTTTAAAAACATATCTGCTAACAA-TACAGTTG-3'), 5' arm antisense (5'-AGGCCGGCCAAAGGAT-CCATAACTTCGTATAGCATACATTATACGAAGTTATCGAGCCC-CAAATCCAACCTTTACCAG-3'), Exon14-16 sense (5'-AGGATCCGGT-GCCCTACTCAAATCTCCAATGC-3'), exon 14-16 antisense (5'-AGGC-CGGCCATAACTTCGTATAGCATACATTATACGAAGTTATAGC-TGGAGACCTGGTGGCAGTCCTG-3'), splice donor sense (5'-AACCGGTGTGCCATGCCAGCCATGGTACCTCACCATG-3'), splice donor antisense (5'-TACCGGTTAATTAACATATGTAGCTGGAGACCTG-GTGGCAGTCCTG-3'), 3' arm sense (5'-TGGCGCGCCATATGG-AGTACCATCGGCTGCCGAGTCAGCTC-3'), and 3' arm antisense (5'-ACTCGAGTCGACGATCCCTGATCTCTTGCCCTCCTCCAC-3').

Primers used for screening and routine genotyping are as follows: P1 5' LoxP sense (5'-ATCCAACCTCTCCAGCCAATAACC-3'), P2 5' LoxP antisense (5'-GAGGCGTGTGGAAGTCTGC-3'), P3 mRNA sense (5'-CGTTGTGAGTTGGATAGTTGTGG-3'), P4 mRNA antisense (5'-AGCTGGCTCTGAAAGATGAAGG-3'), P5 3' LoxP sense (5'-CCTA-TCCCTATGCCTACCCACCCATG-3'), P6 3' LoxP antisense (5'-AGC-TGACTCGGCAGCCGATGGTACTC-3'), and P7 *neo*-IRES sense (5'-CGTATTCAACAAGGGGCTGAAGGATGC-3'). All animals were maintained in specific pathogen-free conditions consistent with EU and UK regulations. All the work was performed under a UK Home Office project license that was awarded after recommendation by the University of Dundee Ethical Review Committee. The ABIN1[D485N] mice generated were on a 129SvJ \times C57BL/6 background and were backcrossed two generations to C57BL/6. MyD88^{-/-} mice were provided by S. Akira (Osaka University, Osaka, Japan) and RIP2^{-/-} mice were obtained from R.A. Flavell (Yale University School of Medicine, New Haven, CT).

Flow cytometry. Single-cell suspensions were made from thymus and spleen by gentle sieving and pipetting, whereas BM samples were prepared by flushing them out from tibia and femur with PBS. Peritoneal lavage was collected by injecting 10 ml PBS into the peritoneum. Erythrocytes were removed from spleen, BM, and peritoneal lavage by treatment with red blood cell lysis buffer (Sigma-Aldrich). For surface staining, cells were washed twice with ice-cold PBS, 2% (wt/vol) BSA, and 0.1% (wt/vol) sodium azide. 10⁶ cells were blocked for 15 min with Fc γ antibody (purified CD16/32; 2.4G2; BD) and incubated for 30 min at 4°C with various antibodies conjugated to FITC, phycoerythrin (PE), PE-Cy5 (Tricolor), APC, or APC-Cy7 for multiple color fluorescence surface staining. For analysis of various cell types, cell surface markers examined included (with clone numbers in parentheses) Thy1.2 (53-2.1), CD45R (B220; RA3-6B2), CD4 (RM4-5), CD8 α (53-6.7), TCR- β (H57-597), CD86 (GL1), MHC II (M5/114.15.2), CD44

(IM7), CD62L (MEL-14), CD69 (H1.2F3), CD138 (syndecan-1, 281-2), CD40 (3/23), CD43 (S7), Gr-1 (Ly6C/G; RB6-8C5), CD11c (HL3), CD5 (53-7.3), CD21 (7G6), CD23 (B3B4), CD25 (PC61.5), IgM (II/41), CXCR5 (2G8), PD-1 (J43), and GL-7 CD95 (Jo2; all antibodies were obtained from BD). CD11b and F4/80 antibodies were obtained from Invitrogen. The mouse T reg cell detection kit (FJK-16s) was obtained from eBioscience. Data were acquired with a FACSCalibur (BD) flow cytometer with Cell Quest software. Results were analyzed with FlowJo software (Tree Star).

Histopathology and immunohistochemistry. Formalin-fixed tissues were stained with hematoxylin & eosin or with the PAS reagent. For immunohistochemical labeling of germinal centers, sections were dewaxed in xylene and rehydrated through graded alcohols. Proteinase K (Dako) was applied for 20 min at 20°C for antigen retrieval, and slides were washed in buffer and a peroxidase blocker applied (Dako) for 5 min, followed by further washes. The slides were incubated for 1 h with biotinylated peanut agglutinin (Vector Laboratories) diluted 1:100. After washing, Avidin-Biotin Complex was applied for 30 min, washed again, and visualized by incubation for two 5-min periods in diaminobenzidine (Dako). After further washing, counterstaining was performed for 30 s using Gill's hematoxylin. Stained sections were washed, dehydrated, and mounted under glass coverslips with DPX. For immunofluorescence studies, kidney sections were washed three times in PBS and blocked for 30 min at 20°C with 2.5% horse serum, 1% BSA, 0.05% Tween 20, and 0.05% Triton X-100. Sections were washed three times in PBS and mounted with Vectashield. FITC conjugated anti-mouse C3 (CL7503F; Cedarlane Laboratories Limited), C1q (JL-1; Hycult Biotech), and IgG (F2266; Sigma-Aldrich) were used for immunostaining. Images were taken on a microscope (BX51; Olympus) with a camera (DP71; Olympus) fitted using acquisition software (Olympus). Images were processed with Photoshop software (CS3; Adobe).

Measurement of autoantibodies and immunoglobulin isotypes by ELISA. Blood was collected from mice by cardiac puncture, allowed to clot, and the serum was separated by centrifugation. Immunoglobulins (Immunology Consultants Laboratory) and autoantibodies to dsDNA and antinuclear antibodies (total Ig; Alpha Diagnostics International) were measured by ELISA.

Multiplex cytokine assays. Cytokines in cell culture supernatants and mouse serum were measured using either Luminex-based Bio-Plex Mouse Grp 1 Cytokine 8-Plex, 6-Plex Panel, or 13 plex (Bio-Rad Laboratories) or individual Bioplex cytokine kits.

B cell and T cell proliferation. Untouched naive splenic B cells of >98% purity were isolated using a B cell isolation kit (Miltenyi Biotec) and 10^5 cells were cultured for 72 h in 96-well plates with LPS and LTA, R848, anti-IgM (Jackson ImmunoResearch Laboratories, Inc.), or anti-CD40 (Clone 3/23; BD). Splenic and LN CD4⁺ T cells (>95% pure) were isolated using a CD4⁺ T cell isolation kit (Miltenyi Biotec) and stimulated for 72 h with plate-bound anti-CD3 alone (clone 145-2C11; BD) or with anti-CD3 plus anti-CD28 (37.51; BD). The samples were pulsed for 16 h with 0.5 μ Ci [³H]thymidine before harvesting and measuring [³H]thymidine incorporation.

Generation of BMDM and BMDC. BMDM and BMDC were obtained by differentiating femur and tibia BM using recombinant mouse M-CSF (R&D Systems) and GM-CSF (R&D Systems), respectively. After 12–24 h of replating, cells were stimulated with LPS (*Escherichia coli* strain O5:B55; Enzo Life Sciences), LTA from *Staphylococcus aureus*, Pam3CSK4, CpG DNA (ODN 1826), or R848 (TLR7 agonist), all obtained from InvivoGen. For immunoprecipitation and immunoblotting, cell extracts were prepared as previously described (Windheim et al., 2008).

Immunoblotting and immunoprecipitation. 10 μ g of cell extract protein was subjected to SDS-PAGE and immunoblotting as previously described (Windheim et al., 2008). To immunoprecipitate ABIN1, 1.0 mg of cell extract protein was incubated for 2 h with 0.5 μ g of the ABIN1 antibody.

After mixing end over end for 60 min with 15 μ l of protein G-Agarose beads, the agarose was collected and washed six times with cell lysis buffer plus 0.5 M NaCl. Immunoprecipitates were denatured in SDS, subjected to SDS-PAGE, and immunoblotted.

Antibodies for immunoblotting and immunoprecipitation. Sheep antibodies against mouse ABIN1 (sheep number S345C, third bleed) and human TAK1 (sheep number S828A, first bleed) were generated in the MRC Protein Phosphorylation Unit by J. Hastie (University of Dundee, Dundee, UK). Antibodies that recognize IKK- α/β phosphorylated at Ser180/Ser181 or Ser 176/180, p105/NF- κ B1 phosphorylated at Ser933, p38 MAPK phosphorylated at the TGY motif, ERK1/ERK2 phosphorylated at the TEY motif, I κ B α phosphorylated at Ser32/36, and antibodies that recognize the deubiquitylase A20, all forms of p38 MAPK, ERK1/ERK2, I κ B α , Caspase8, and Caspase3 were obtained from Cell Signaling Technology. JNK phosphorylated at the TPY motif was from Invitrogen. Mouse monoclonal antibodies against GAPDH (Abcam) and ubiquitin (P4D1; Santa Cruz Biotechnology, Inc.), anti-IRAK1 (Santa Cruz Biotechnology, Inc.), and rabbit-, mouse-, and sheep-specific secondary antibodies conjugated to horseradish peroxidase (Thermo Fisher Scientific) were purchased from the suppliers in parentheses.

Measurement of TAK1 activity. This was performed as described previously (Cheung et al., 2003), except that α -TAK1 was used to immunoprecipitate TAK1 instead of α -TAB1. In brief, TAK1 complexes were immunoprecipitated from 0.15 mg BMDC extract protein, using 0.45 μ g anti-TAK1 antibody. The TAK1 activity in the immunoprecipitates was measured by the activation of MAPK kinase 6 and coupled to the activation of p38 α MAPK. The active p38 α MAPK generated in this step was quantified in a second assay by measuring its ability to incorporate [³²P]-phosphate from γ -[³²P]ATP into myelin basic protein.

Statistical analysis. Statistical significance was calculated either using the two-tailed Student's *t* test or the Mann-Whitney *U* test using Prism software (GraphPad Software). Further details are provided in the relevant figure legends.

Online supplemental material. Fig. S1 shows design of the targeting vector and the expression pattern of ABIN1 protein in various cells from ABIN1[D485N] mice. Fig. S2 shows immune phenotyping of ABIN1[D485N] mice. Fig. S3 shows no alteration in T cell receptor signaling in ABIN1 knockin mice. Fig. S4 shows enhanced activation of LPS signaling in B cells and also enhanced activation of TLR-MyD88 and NOD1-RIP2 signaling pathways in BMDM from ABIN1[D485N] mice. Fig. S5 shows rescue of the T cell phenotype observed in ABIN1[D485N]/MyD88^{-/-} mice. Fig. S6 shows enhanced activated of TLR signaling in BMDM from ABIN1[Δ478–606] mice, the phenotype of ABIN1[Δ478–606] mice, and enhanced TNF-induced apoptosis in embryonic fibroblasts from ABIN1[D485N] mice. Fig. S7 shows TNF and IL-1 signaling in embryonic fibroblasts from ABIN1[D485N] mice. Online supplemental material is available at <http://www.jem.org/cgi/content/full/jem.20102177/DC1>.

We thank S. Akira (Osaka University, Japan) for MyD88^{-/-} mice, R.A. Flavell (Yale University) for RIP2^{-/-} mice, J. Hastie (University of Dundee, UK) for generating and purifying the ABIN1 and TAK1 antibodies, S. Walsh (University of Dundee) and A. Philby (University of Glasgow) for preliminary pathological analysis of tissues, E. Wright (University of Dundee) for blood and BM analysis, M. Peggie for DNA cloning, S. Conner and M. Windheim for initial studies of polyubiquitin binding to ABIN1 and NEMO, and P. Crocker (University of Dundee) for helpful discussions. We thank the Transgenic Mouse Facility at the University of Dundee for help in generating ABIN1[D485N] mice and D.W. Freeman, M.B. Knights, and M.N. Lowry for technical assistance with kidney immunofluorescence experiments.

This study was supported by grants from the UK Medical Research Council and The Royal Society (to P. Cohen), an MRC Studentship (to A. Ordureau), and US National Institutes of Health Grant DK 176743 (to D.W. Powell).

The authors have no conflicting financial interests.

Submitted: 13 October 2010

Accepted: 25 April 2011

REFERENCES

- Banchereau, J., and V. Pascual. 2006. Type I interferon in systemic lupus erythematosus and other autoimmune diseases. *Immunity*. 25:383–392. doi:10.1016/j.immuni.2006.08.010
- Bessa, J., M. Kopf, and M.F. Bachmann. 2010. Cutting edge: IL-21 and TLR signaling regulate germinal center responses in a B cell-intrinsic manner. *J. Immunol.* 184:4615–4619. doi:10.4049/jimmunol.0903949
- Boone, D.L., E.E. Turer, E.G. Lee, R.C. Ahmad, M.T. Wheeler, C. Tsui, P. Hurley, M. Chien, S. Chai, O. Hitotsumatsu, et al. 2004. The ubiquitin-modifying enzyme A20 is required for termination of Toll-like receptor responses. *Nat. Immunol.* 5:1052–1060. doi:10.1038/ni1110
- Cheung, P.C., D.G. Campbell, A.R. Nebreda, and P. Cohen. 2003. Feedback control of the protein kinase TAK1 by SAPK2a/p38alpha. *EMBO J.* 22:5793–5805. doi:10.1093/emboj/cdg552
- Chu, Y., J.C. Vahl, D. Kumar, K. Heger, A. Bertossi, E. Wójciewicz, V. Soberon, D. Schenten, B. Mack, M. Reutelschöfer, et al. 2011. B cells lacking the tumor suppressor TNFAIP3/A20 display impaired differentiation and hyperactivation and cause inflammation and autoimmunity in aged mice. *Blood*. 117:2227–2236. doi:10.1182/blood-2010-09-306019
- Conze, D.B., C.J. Wu, J.A. Thomas, A. Landstrom, and J.D. Ashwell. 2008. Lys63-linked polyubiquitination of IRAK-1 is required for interleukin-1 receptor- and toll-like receptor-mediated NF-kappaB activation. *Mol. Cell. Biol.* 28:3538–3547. doi:10.1128/MCB.02098-07
- Döffinger, R., A. Smahi, C. Bessia, F. Geissmann, J. Feinberg, A. Durandy, C. Bodemer, S. Kenwrick, S. Dupuis-Girod, S. Blanche, et al. 2001. X-linked anhidrotic ectodermal dysplasia with immunodeficiency is caused by impaired NF-kappaB signaling. *Nat. Genet.* 27:277–285. doi:10.1038/85837
- Ea, C.K., L. Deng, Z.P. Xia, G. Pineda, and Z.J. Chen. 2006. Activation of IKK by TNFalpha requires site-specific ubiquitination of RIP1 and polyubiquitin binding by NEMO. *Mol. Cell.* 22:245–257. doi:10.1016/j.molcel.2006.03.026
- El Bakkouri, K., A. Wullaert, M. Haegman, K. Heynink, and R. Beyaert. 2005. Adenoviral gene transfer of the NF-kappa B inhibitory protein ABIN-1 decreases allergic airway inflammation in a murine asthma model. *J. Biol. Chem.* 280:17938–17944. doi:10.1074/jbc.M413588200
- Haas, T.L., C.H. Emmerich, B. Gerlach, A.C. Schmukle, S.M. Cordier, E. Rieser, R. Feltham, J. Vince, U. Warnken, T. Wenger, et al. 2009. Recruitment of the linear ubiquitin chain assembly complex stabilizes the TNF-R1 signaling complex and is required for TNF-mediated gene induction. *Mol. Cell.* 36:831–844. doi:10.1016/j.molcel.2009.10.013
- Han, J.W., H.F. Zheng, Y. Cui, L.D. Sun, D.Q. Ye, Z. Hu, J.H. Xu, Z.M. Cai, W. Huang, G.P. Zhao, et al. 2009. Genome-wide association study in a Chinese Han population identifies nine new susceptibility loci for systemic lupus erythematosus. *Nat. Genet.* 41:1234–1237. doi:10.1038/ng.472
- He, B., R. Santamaria, W. Xu, M. Cols, K. Chen, I. Puga, M. Shan, H. Xiong, J.B. Bussel, A. Chiu, et al. 2010a. The transmembrane activator TACI triggers immunoglobulin class switching by activating B cells through the adaptor MyD88. *Nat. Immunol.* 11:836–845. doi:10.1038/ni.1914
- He, C.F., Y.S. Liu, Y.L. Cheng, J.P. Gao, T.M. Pan, J.W. Han, C. Quan, L.D. Sun, H.F. Zheng, X.B. Zuo, et al. 2010b. TNIP1, SLC15A4, ETS1, RasGRP3 and IKZF1 are associated with clinical features of systemic lupus erythematosus in a Chinese Han population. *Lupus*. 19:1181–1186. doi:10.1177/0961203310367918
- Heynink, K., D. De Valck, W. Vanden Berghe, W. Van Criekinge, R. Contreras, W. Fiers, G. Haegeman, and R. Beyaert. 1999. The zinc finger protein A20 inhibits TNF-induced NF-kB-dependent gene expression by interfering with an RIP- or TRAF2-mediated transactivation signal and directly binds to a novel NF-kB-inhibiting protein ABIN. *J. Cell Biol.* 145:1471–1482. doi:10.1083/jcb.145.7.1471
- Heynink, K., M.M. Kreike, and R. Beyaert. 2003. Structure-function analysis of the A20-binding inhibitor of NF-kappa B activation, ABIN-1. *FEBS Lett.* 536:135–140. doi:10.1016/S0014-5793(03)00041-3
- Hwang, I.Y., C. Park, K. Harrison, and J.H. Kehrl. 2009. TLR4 signaling augments B lymphocyte migration and overcomes the restriction that limits access to germinal center dark zones. *J. Exp. Med.* 206:2641–2657. doi:10.1084/jem.20091982
- Inohara, N., M. Chamaillard, C. McDonald, and G. Nuñez. 2005. NOD-LRR proteins: role in host-microbial interactions and inflammatory disease. *Annu. Rev. Biochem.* 74:355–383. doi:10.1146/annurev.biochem.74.082803.133347
- Kanayama, A., R.B. Seth, L. Sun, C.K. Ea, M. Hong, A. Shaito, Y.H. Chiu, L. Deng, and Z.J. Chen. 2004. TAB2 and TAB3 activate the NF-kappaB pathway through binding to polyubiquitin chains. *Mol. Cell.* 15:535–548. doi:10.1016/j.molcel.2004.08.008
- Kawagoe, T., O. Takeuchi, Y. Takabatake, H. Kato, Y. Isaka, T. Tsujimura, and S. Akira. 2009. TANK is a negative regulator of Toll-like receptor signaling and is critical for the prevention of autoimmune nephritis. *Nat. Immunol.* 10:965–972. doi:10.1038/ni.1771
- Kirisako, T., K. Kamei, S. Murata, M. Kato, H. Fukumoto, M. Kanie, S. Sano, F. Tokunaga, K. Tanaka, and K. Iwai. 2006. A ubiquitin ligase complex assembles linear polyubiquitin chains. *EMBO J.* 25:4877–4887. doi:10.1038/sj.emboj.7601360
- Komander, D., F. Reyes-Turcu, J.D. Licchesi, P. Odenwaelde, K.D. Wilkinson, and D. Barford. 2009. Molecular discrimination of structurally equivalent Lys 63-linked and linear polyubiquitin chains. *EMBO Rep.* 10:466–473. doi:10.1038/embor.2009.55
- Kulathu, Y., M. Akutsu, A. Bremm, K. Hofmann, and D. Komander. 2009. Two-sided ubiquitin binding explains specificity of the TAB2 NZF domain. *Nat. Struct. Mol. Biol.* 16:1328–1330. doi:10.1038/nsmb.1731
- Ma, C.S., S. Suryani, D.T. Avery, A. Chan, R. Nanan, B. Santner-Nanan, E.K. Deenick, and S.G. Tangye. 2009. Early commitment of naïve human CD4(+) T cells to the T follicular helper (T(FH)) cell lineage is induced by IL-12. *Immunol. Cell Biol.* 87:590–600. doi:10.1038/icb.2009.64
- Marshak-Rothstein, A. 2006. Toll-like receptors in systemic autoimmune disease. *Nat. Rev. Immunol.* 6:823–835. doi:10.1038/nri1957
- Nair, R.P., K.C. Duffin, C. Helms, J. Ding, P.E. Stuart, D. Goldgar, J.E. Gudjonsson, Y. Li, T. Tejasvi, B.J. Feng, et al; Collaborative Association Study of Psoriasis. 2009. Genome-wide scan reveals association of psoriasis with IL-23 and NF-kappaB pathways. *Nat. Genet.* 41:199–204. doi:10.1038/ng.311
- Nurieva, R.I., Y. Chung, D. Hwang, X.O. Yang, H.S. Kang, L. Ma, Y.H. Wang, S.S. Watowich, A.M. Jetten, Q. Tian, and C. Dong. 2008. Generation of T follicular helper cells is mediated by interleukin-21 but independent of T helper 1, 2, or 17 cell lineages. *Immunity*. 29:138–149. doi:10.1016/j.immuni.2008.05.009
- Ordureau, A., H. Smith, M. Windheim, M. Pegg, E. Carrick, N. Morrice, and P. Cohen. 2008. The IRAK-catalysed activation of the E3 ligase function of Pellino isoforms induces the Lys63-linked polyubiquitination of IRAK1. *Biochem. J.* 409:43–52. doi:10.1042/BJ20071365
- Oshima, S., E.E. Turer, J.A. Callahan, S. Chai, R. Advincula, J. Barrera, N. Shifrin, B. Lee, T.S. Benedict, T. Woo, et al. 2009. ABIN-1 is a ubiquitin sensor that restricts cell death and sustains embryonic development. *Nature*. 457:906–909. doi:10.1038/nature07575
- Pasare, C., and R. Medzhitov. 2004. Toll-dependent control mechanisms of CD4 T cell activation. *Immunity*. 21:733–741. doi:10.1016/j.immuni.2004.10.006
- Peng, G., Z. Guo, Y. Kiniwa, K.S. Voo, W. Peng, T. Fu, D.Y. Wang, Y. Li, H.Y. Wang, and R.F. Wang. 2005. Toll-like receptor 8-mediated reversal of CD4+ regulatory T cell function. *Science*. 309:1380–1384. doi:10.1126/science.1113401
- Plenge, R.M., C. Cotsapas, L. Davies, A.L. Price, P.I. de Bakker, J. Maller, I. Pe'er, N.P. Burt, B. Blumenstiel, M. DeFelice, et al. 2007. Two independent alleles at 6q23 associated with risk of rheumatoid arthritis. *Nat. Genet.* 39:1477–1482. doi:10.1038/ng.2007.27
- Rahighi, S., F. Ikeda, M. Kawasaki, M. Akutsu, N. Suzuki, R. Kato, T. Kensche, T. Uejima, S. Bloor, D. Komander, et al. 2009. Specific recognition of linear ubiquitin chains by NEMO is important for NF-kappaB activation. *Cell*. 136:1098–1109. doi:10.1016/j.cell.2009.03.007
- Sato, S., H. Sanjo, K. Takeda, J. Ninomiya-Tsuji, M. Yamamoto, T. Kawai, K. Matsumoto, O. Takeuchi, and S. Akira. 2005. Essential function for the kinase TAK1 in innate and adaptive immune responses. *Nat. Immunol.* 6:1087–1095. doi:10.1038/ni1255
- Sato, Y., A. Yoshikawa, M. Yamashita, A. Yamagata, and S. Fukui. 2009. Structural basis for specific recognition of Lys 63-linked polyubiquitin

- chains by NZF domains of TAB2 and TAB3. *EMBO J.* 28:3903–3909. doi:10.1038/emboj.2009.345
- Schmitt, N., R. Morita, L. Bourdery, S.E. Bentebibel, S.M. Zurawski, J. Banchereau, and H. Ueno. 2009. Human dendritic cells induce the differentiation of interleukin-21-producing T follicular helper-like cells through interleukin-12. *Immunity*. 31:158–169. doi:10.1016/j.immuni.2009.04.016
- Shim, J.H., C. Xiao, A.E. Paschal, S.T. Bailey, P. Rao, M.S. Hayden, K.Y. Lee, C. Bussey, M. Steckel, N. Tanaka, et al. 2005. TAK1, but not TAB1 or TAB2, plays an essential role in multiple signaling pathways in vivo. *Genes Dev.* 19:2668–2681. doi:10.1101/gad.1360605
- Sutmoller, R., A. Garritsen, and G.J. Adema. 2007. Regulatory T cells and toll-like receptors: regulating the regulators. *Ann. Rheum. Dis.* 66:iii91–iii95. doi:10.1136/ard.2007.078535
- Tavares, R.M., E.E. Turer, C.L. Liu, R. Advincula, P. Scapini, L. Rhee, J. Barrera, C.A. Lowell, P.J. Utz, B.A. Malynn, and A. Ma. 2010. The ubiquitin modifying enzyme A20 restricts B cell survival and prevents autoimmunity. *Immunity*. 33:181–191. doi:10.1016/j.immuni.2010.07.017
- Thomson, W., A. Barton, X. Ke, S. Eyre, A. Hinks, J. Bowes, R. Donn, D. Symmons, S. Hider, I.N. Bruce, et al; Wellcome Trust Case Control Consortium; YEAR Consortium. 2007. Rheumatoid arthritis association at 6q23. *Nat. Genet.* 39:1431–1433. doi:10.1038/ng.2007.32
- Tokunaga, F., S. Sakata, Y. Saeki, Y. Satomi, T. Kirisako, K. Kamei, T. Nakagawa, M. Kato, S. Murata, S. Yamaoka, et al. 2009. Involvement of linear polyubiquitylation of NEMO in NF-kappaB activation. *Nat. Cell Biol.* 11:123–132. doi:10.1038/ncb1821
- Vinuesa, C.G., M.C. Cook, C. Angelucci, V. Athanasopoulos, L. Rui, K.M. Hill, D. Yu, H. Domasch, B. Whittle, T. Lambe, et al. 2005. A RING-type ubiquitin ligase family member required to repress follicular helper T cells and autoimmunity. *Nature*. 435:452–458. doi:10.1038/nature03555
- Vinuesa, C.G., I. Sanz, and M.C. Cook. 2009. Dysregulation of germinal centres in autoimmune disease. *Nat. Rev. Immunol.* 9:845–857. doi:10.1038/nri2637
- Wagner, S., I. Carpentier, V. Rogov, M. Kreike, F. Ikeda, F. Löhr, C.J. Wu, J.D. Ashwell, V. Dötsch, I. Dikic, and R. Beyaert. 2008. Ubiquitin binding mediates the NF-kappaB inhibitory potential of ABIN proteins. *Oncogene*. 27:3739–3745. doi:10.1038/sj.onc.1211042
- Walsh, M.C., G.K. Kim, P.L. Maurizio, E.E. Molnar, and Y. Choi. 2008. TRAF6 autoubiquitination-independent activation of the NFkappaB and MAPK pathways in response to IL-1 and RANKL. *PLoS ONE*. 3:e4064. doi:10.1371/journal.pone.0004064
- Wang, C., L. Deng, M. Hong, G.R. Akkaraju, J. Inoue, and Z.J. Chen. 2001. TAK1 is a ubiquitin-dependent kinase of MKK and IKK. *Nature*. 412:346–351. doi:10.1038/35085597
- Wertz, I.E., K.M. O'Rourke, H. Zhou, M. Eby, L. Aravind, S. Seshagiri, P. Wu, C. Wiesmann, R. Baker, D.L. Boone, et al. 2004. De-ubiquitination and ubiquitin ligase domains of A20 downregulate NF-kappaB signalling. *Nature*. 430:694–699. doi:10.1038/nature02794
- Windheim, M., C. Lang, M. Pegg, L.A. Plater, and P. Cohen. 2007. Molecular mechanisms involved in the regulation of cytokine production by muramyl dipeptide. *Biochem. J.* 404:179–190. doi:10.1042/BJ20061704
- Windheim, M., M. Stafford, M. Pegg, and P. Cohen. 2008. Interleukin-1 (IL-1) induces the Lys63-linked polyubiquitination of IL-1 receptor-associated kinase 1 to facilitate NEMO binding and the activation of IkappaBalpha kinase. *Mol. Cell. Biol.* 28:1783–1791. doi:10.1128/MCB.02380-06
- Wu, C.J., D.B. Conze, T. Li, S.M. Srinivasula, and J.D. Ashwell. 2006. Sensing of Lys 63-linked polyubiquitination by NEMO is a key event in NF-kappaB activation [corrected]. *Nat. Cell Biol.* 8:398–406. doi:10.1038/ncb1384
- Xia, Z.P., L. Sun, X. Chen, G. Pineda, X. Jiang, A. Adhikari, W. Zeng, and Z.J. Chen. 2009. Direct activation of protein kinases by unanchored polyubiquitin chains. *Nature*. 461:114–119. doi:10.1038/nature08247